ORNL-TM-4131

CREEP PROPERTIES OF A TYPE 308 STAINLESS STEEL PRESSURE VESSEL WELD WITH CONTROLLED RESIDUAL ELEMENTS

R. T. King
J. O. Stiegler
G. M. Goodwin

OAK RIDGE NATIONAL LABORATORY
OPERATED BY UNION CARBIDE CORPORATION • FOR THE U.S. ATOMIC ENERGY COMMISSION

DISCLAIMER

Printed in the United States of America. Available from
National Technical Information Service
U.S. Department of Commerce
5285 Port Royal Road, Springfield, Virginia 22151
Price: Printed Copy ~~$3.00~~ 4.00; Microfiche $0.95

ORNL-TM-4131
UC-79b — Liquid Metal Fast Breeder Reactors
(Fuels and Materials Engineering and Development)

Contract No. W-7405-eng-26

METALS AND CERAMICS DIVISION

CREEP PROPERTIES OF A TYPE 308 STAINLESS STEEL PRESSURE VESSEL WELD WITH CONTROLLED RESIDUAL ELEMENTS

R. T. King, J. O. Stiegler, and G. M. Goodwin

Based on a paper submitted to the International Conference on Creep and Fatigue in Elevated Temperature Applications, Philadelphia, Pennsylvania, September 23–28, 1973.

MAY 1973

OAK RIDGE NATIONAL LABORATORY
Oak Ridge, Tennessee 37830
operated by
UNION CARBIDE CORPORATION
for the
U.S. ATOMIC ENERGY COMMISSION

THIS PAGE

WAS INTENTIONALLY

LEFT BLANK

CONTENTS

CREEP PROPERTIES OF A TYPE 308 STAINLESS STEEL PRESSURE VESSEL WELD WITH CONTROLLED RESIDUAL ELEMENTS

R. T. King, J. O. Stiegler, and G. M. Goodwin

ABSTRACT

A SMA type 308 stainless steel pressure vessel test weld with the controlled residual elements (CRE) boron (0.007%), titanium (0.06%), and phosphorus (0.04%) was tested in creep between 482 and 650°C (900 and 1200°F). Improved ductility compared to that of standard welds in tests lasting several thousands of hours is associated with the absence of interphase separation. Systematic variations of microstructure and creep properties through the weld and in the heat-affected zone are due to thermal and mechanical cycling during the welding process. Anisotropic deformation occurs and is related to local substructure and preferred crystallographic orientation. Creep strengths are acceptable by present design rules.

INTRODUCTION

The incipient use of pressure vessels and primary components for power stations in the creep deformation range raises several problems. Therefore, more detailed consideration is being given to deformation in such systems than is normally accorded to systems operating at lower temperatures. The behavior of sound welds under the complex thermal and stress histories[1] that they will experience is not yet well understood. Present design rules[2] for nuclear components operating above 427°C (800°F) allow the use of base metal properties in place of weld metal properties, but reduce the allowed deformation of weld metal to one-half that permitted for the base metal. These rules do not

[1]A. C. Gangadharan, "Design and Analysis Experience with a Liquid Metal Heat Exchanger for FFTF Service," paper presented at the 93rd Winter Annual Meeting of the ASME, New York, November 26—30, 1972.

[2]Case 1331-6, *Interpretations of ASME Boiler and Pressure Vessel Code*, American Society of Mechanical Engineers, New York, 1972.

explicitly account for the stress concentrations that can occur near welds nor for the inherent differences between weld metal and base metal properties. Interactions between these factors have been shown to play an important role in the behavior of weld joints.[3]

Welds are generally heterogeneous structures, which result from joining two components with fused metal. There are numerous acceptable methods for generating heat, adding filler metal, and limiting the reactions of the molten metal with its environment. Any variations in the materials and welding process can affect the structure and properties of the finished weldment.

Thick sections of type 304 stainless steel plate are commonly joined with type 308 stainless steel weld metal. A wide range of ductility values for type 308 stainless steel is reported, but the greatest values at any rupture time decrease with increasing rupture time. Strains as low as 1% have been reported[4,5] from uniaxial creep tests for rupture times up to 10,000 hr at temperatures above 565°C (1050°F). Over a 20-year component service life, it is not certain that type 308 stainless steel welds are capable of straining up to the limits of the design rules without failing when the welds are indeed stressed.

The problem of low long-time creep ductility of type 308 stainless steel weld metal has been attacked in a weld development program by studying the effects of minor chemical composition variations on

---

[3]D. J. Walters, T. Rowley, and W. J. Elder, "The Creep Assessment of Butt Welded Pipes and Tubes," paper presented at International Conference on Welding Research Related to Power Plant, September 17–21, 1972, Central Electricity Generating Board Marchwood Engineering Laboratories, England.

[4]H. R. Voorhees and J. W. Freeman, *The Elevated-Temperature Properties of Weld-Deposited Metal and Weldments, ASTM Spec. Tech. Publ.* 226, American Society For Testing and Materials, Philadelphia, 1958.

[5]N. W. Davis and T. M. Cullen, "The Influence of Nitrogen Content on the Rupture Properties of Type 308 Stainless Steel Weldments," pp. 54–65 in *Symposium on Properties of Weldments at Elevated Temperatures April 1968, Chicago,* ed. by M. Semchyshen, American Society of Mechanical Engineers, New York.

ductility.[6-9] Although other variables and welding parameters are also important,[10] the amounts of boron, phosphorus, and titanium in the deposited weld metal are among the most important factors noted that influence the creep ductility of type 308 stainless steel weld metal. A subclass of this type weld metal, which contains 0.007% B, 0.06% Ti, and 0.04% P, has been unofficially designated CRE type 308 stainless steel for the controlled residual elements (CRE) that it contains.

Thick-section plate welds of CRE type 308 stainless steel have been made by a commercial vendor and are presently undergoing extensive tensile, creep, and stress-relaxation testing. The tests have two major aims: first, to obtain design data, and second, to verify the improved long-term creep ductility of the CRE weld metal found in the weld development program.

This report summarizes the creep test results and the results of metallographic studies of the as-welded plates and tested specimens. Large systematic variations in mechanical properties occurred through the thickness of the test welds. These variations result from systematic variations of microstructural features and, perhaps, local chemical composition variations. Another feature of the welds that complicates analysis of their behavior is anisotropy of deformation. These aspects of weld deformation were investigated for the test welds.

---

[6]G. M. Slaughter, N. C. Binkley, G. M. Goodwin, D. G. Harman, and N. C. Cole, *Metals and Ceramics Div. Annu. Progr. Rep. June 30, 1970,* ORNL-4570, pp. 88–91.

[7]G. M. Goodwin, N. C. Binkley, N. C. Cole, and R. G. Bergren, *Metals and Ceramics Div. Annu. Progr. Rep. June 30, 1971,* ORNL-4770, pp. 82–85.

[8]A. J. Moorhead and D. A. Canonico, *Metals and Ceramics Div. Annu. Progr. Rep. June 30, 1971,* ORNL-4770, pp. 129–30.

[9]G. M. Goodwin, N. C. Cole, and R. G. Berggren, *Metals and Ceramics Div. Annu. Progr. Rep. June 30, 1972,* ORNL-4820, pp. 73–75.

[10]G. M. Goodwin, N. C. Cole, and G. M. Slaughter, "A Study of Ferrite Morphology in Austenitic Stainless Steel Weldments," *Welding J. (Miami)* 51(9): 425s–429s (September 1972).

EXPERIMENTAL PROCEDURES

Specimen Preparation

The experimental program includes test welds made by a commercial vendor from four batches of CRE type 308 stainless steel electrodes and two heats of type 304 stainless steel base metal. The chemical compositions of the deposited weld metal and base metal are given in Table 1.

The SMA test welds were made by manually joining 15 × 20 × 6-cm-thick sections of the stainless steel plates along the 20-cm length with 0.635-cm-diam coated electrodes. The B, P, and Ti contents of the weld were controlled by additions of these elements to the flux coating. The welding current and voltage were 300 A DCRP (direct current, reverse polarity) and 45 V. A both-sides U-groove joint design[11] was used, and constraints prevented the plates from flexing about the weld. The root pass was deposited, excess base metal was removed to assure a full penetration weld, and the grooves were filled with weld metal deposited in about 35 to 40 passes. The final weld is nearly hourglass shaped and almost symmetrical about the midplane of the plate, and it is two passes wide everywhere except at the root.

The mechanical properties testing program involved two types of specimens, a standard specimen with a 0.635-cm-diam by 3.175-cm-long gage section and a "buttonhead" specimen with a 0.317-cm-diam by 2.86-cm-long gage section. Standard specimens were cut from the weld in both longitudinal and transverse directions as shown in Fig. 1. The results justify grouping the specimens according to distance from the nearest plate surface regardless of which side of the midplane they came from. Thus, specimens of the L1, L2, and L3 types and specimens of the T1, T2, and T3 types all have center lines 0.48, 1.42, and 2.39 ± 0.1 cm below the nearest plate surfaces, respectively. The buttonhead specimens were longitudinally oriented at the same distances beneath the plate surface, but they were

---

[11] "Fundamentals of Welding," p. 1.46 in Sect. 1 of the *Welding Handbook*, 6th ed., American Welding Society, New York, 1968.

Table 1. Chemical Composition of Type 304 Stainless Steel Base Metal and Type 308 Stainless Steel Weld Metal Used in Study

Element[a]	Chemical Composition (wt %) of Base Metal from		Chemical Composition (wt %) of Weld Metal from			
	Heat 1	Heat 2	Batch 2	Batch 4	Batch 6	Batch 9
Si	0.64	0.55	0.6	0.52	0.56	0.49
S	0.014	0.011	0.009	0.016	0.005	0.004
P	0.016	0.016	0.042	0.043	0.040	0.044
Mn	1.48	1.60	1.87	1.95	1.83	1.91
C	0.061	0.058	0.061	0.066	0.064	0.061
Cr	18.88	18.68	20.10	19.73	19.70	19.70
Ni	9.56	8.44	10.14	9.88	9.61	9.63
Mo	na[b]	na	0.24	0.25	0.07	0.24
Nb + Ta	na	na	<0.01	0.01	<0.01	<0.01
Ti	na	na	0.06	0.06	0.06	0.06
Co	na	na	0.07	0.07	0.03	0.07
Cu	na	na	0.17	0.16	0.04	0.04
B	na	na	0.007	0.007	0.007	0.007
V	na	na	0.10	0.09	0.07	0.09
N	na	na	0.42	0.039	0.030	0.042

[a] Balance iron.

[b] na = not analyzed.

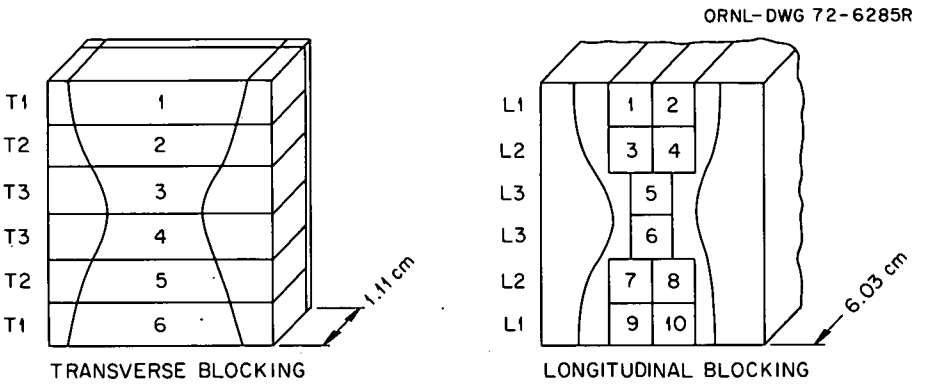

Fig. 1. Location and Orientation of Standard Specimens in the Test Weld. Hourglass-shaped region represents weld metal.

cut from a seven-specimen-across by six-specimen-high square grid. Buttonhead specimens were prepared with gage sections containing all weld metal, all base metal, and part each.

Testing Procedures

Both tensile and creep tests were run on the standard specimens. Nearly all of the standard creep specimens were fitted with averaging extensometers. The measuring sensitivity of the system as it was used was 0.25 μm, and temperatures were controlled to ±3°C along the gage length. The entire strain-time curve was monitored and recorded incrementally with dial gages, but a continuous record of strain versus time was obtained for the early part of the test using linear variable differential transformers (LVDT's). The standard tensile specimens were fitted with averaging extensometers and LVDT's to measure the strains below 2%. The load was measured through a load cell in the pull train. The crosshead deflection-load chart from the Instron tensile testing machine was used for strains from 0.2% to fracture, since it agreed well with the extensometer over this range. Tensile tests were performed at a nominal strain rate of 0.004/min (the tests were not strain-rate controlled) at temperatures between room temperature and 649°C (1200°F). Creep tests were performed at 482, 565, 593, and 649°C (900, 1050, 1100, and 1200°F).

Most buttonhead specimens were tested at 593°C (1100°F) with a nonaveraging extensometer fitted with a dial gage. Most of the specimens were tested under a nominal uniaxial stress of 240 MPa (35,000 psi).

Microscopy Procedures

Optical and electron microscopy were used to study as-received wafers from selected regions of the weld and base metals. Sections were cut parallel and perpendicular to the welding direction. These wafers were thinned electrolytically and examined by transmission electron microscopy to determine the amount of variation that occurred in the microstructure from region to region. Dislocation and precipitate densities were measured quantitatively by stereo techniques to determine foil thickness and dislocation densities in three dimensions. The correction for invisible dislocations was made by assuming all Burgers vectors to be equally probable, an assumption that was verified by examining two or more reflections in some regions.

The fracture surfaces of selected specimens were examined with a scanning electron microscope. The gage sections were then cut to show three orthogonal surfaces in the broken specimen, two parallel and one normal to the load axis. The sections were mounted, polished, and examined metallographically.

RESULTS

Mechanical Properties Results

Extensive tensile testing was done at temperatures of 25, 482, and 592°C (77, 900, and 1100°F). We found no consistent differences at any of these temperatures in properties related to the batch of weld rod or the heats of base plate. The outstanding feature is the variation of properties that occurs through the thickness of the weld. The weld metal from the L1 position near the surface always has yield strengths between 34 and 103 MPa (5,000 and 15,000 psi) lower than weld metal from the L3 position near the center of the weld. Typical results obtained at 482°C (900°F), which indicate the amount of scatter normally encountered in tensile tests, are shown in Fig. 2. Significant reductions in uniform and total ductility always occurred in traversing from the L1 position near the weld surface to the L3 position near the weld center, but the

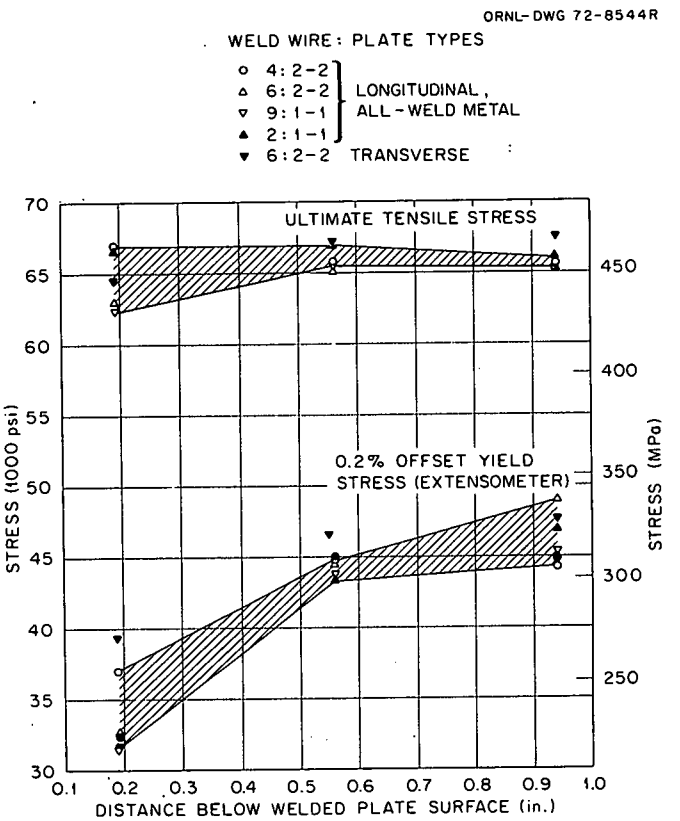

Fig. 2. Tensile Properties of CRE Type 308 Stainless Steel Weld Metal at 482°C and 0.004/min Strain Rate.

uniform and total strains always exceeded 3% and 20%, respectively. No significant variations of ultimate tensile strength with location were observed.

A few transverse tensile specimens were also tested. They usually exhibited higher than average strength (Fig. 2).

Because creep tests were performed at several temperatures, the creep data are conveniently represented by a time-temperature parameter method. The Larson-Miller parameter is used here because of its relative simplicity and widespread acceptance. Other parametric methods are under consideration. Extrapolations of these data using any methods are not presently recommended. Stress is related to the Larson-Miller parameter

by[12]

$$\log_{10}\sigma = f[T(c + \log_{10}t)] \ , \qquad (1)$$

where T is temperature (°R), σ is applied stress (Pa), and the constant c is arbitrarily set equal to 20. The time t refers to several specific identifiable times in a creep test: the time to 0.5% strain ($t_{0.5}$), time to 1% strain ($t_{1.0}$), time to 2% strain ($t_{2.0}$), time to initiation of third-stage creep at a 0.2% offset from steady-state creep (t_3), and time to rupture (t_r). These time data are presented in Figs. 3 through 7, respectively, together with ASME Code Case 1331-6 average values for type 304 stainless steel.[13] All these times were obtained manually from the raw strain-time graphs. Throughout the graphical presentations, the specimen location for each datum is identified. In the case of $t_{0.5}$ (Fig. 3), the results can be separated roughly by specimen location. The differences in behavior of L1, L2, and L3 specimens are more readily distinguished at higher strains for $t_{1.0}$ (Fig. 4) and $t_{2.0}$ (Fig. 5). The time to the onset of third-stage creep for given test conditions (Fig. 6, as determined by a 0.2% strain offset from the minimum creep rate segment of the strain-time plots) is clearly less for L1 specimens than for L2 and L3 specimens. Isothermal data comparisons indicate that the L2 and L3 specimens behave differently, although only one curve is drawn for L2 and L3 specimens on the Larson-Miller plot. This observation also is true of the time-to-rupture plot (Fig. 7). For comparison, the 95% confidence limits for stress to cause rupture for type 304 stainless steel are

---

[12]D. I. Roberts and S. A. Sterling, "A Parametric Method for the Development of Isochronous Stress-Strain Curves," pp. 1–14 in *The Generation of Isochronous Stress-Strain Curves*, ed. by A. O. Schaefer, American Society of Mechanical Engineers, New York, 1972.

[13]Case 1331-6, *Interpretations of ASME Boiler and Pressure Vessel Code*, American Society of Mechanical Engineers, New York, 1972.

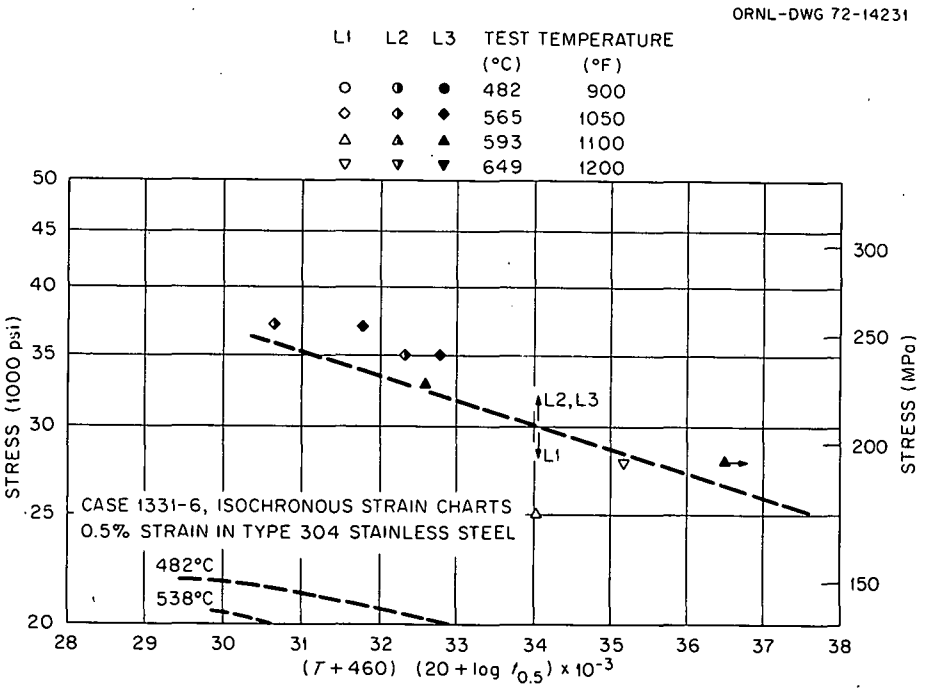

Fig. 3. Stress as a Function of Larson-Miller Parameter for Time to 0.5% Strain in CRE Type 308 Stainless Steel Weld Metal.

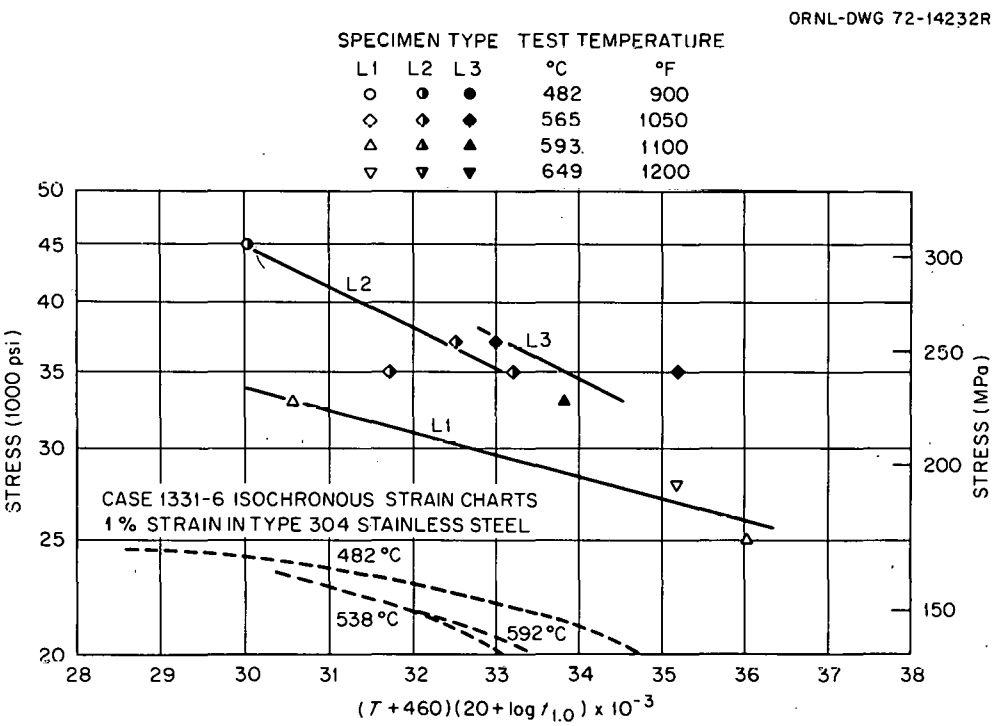

Fig. 4. Stress as a Function of Larson-Miller Parameter for Time to 1% Strain in CRE Type 308 Stainless Steel Weld Metal.

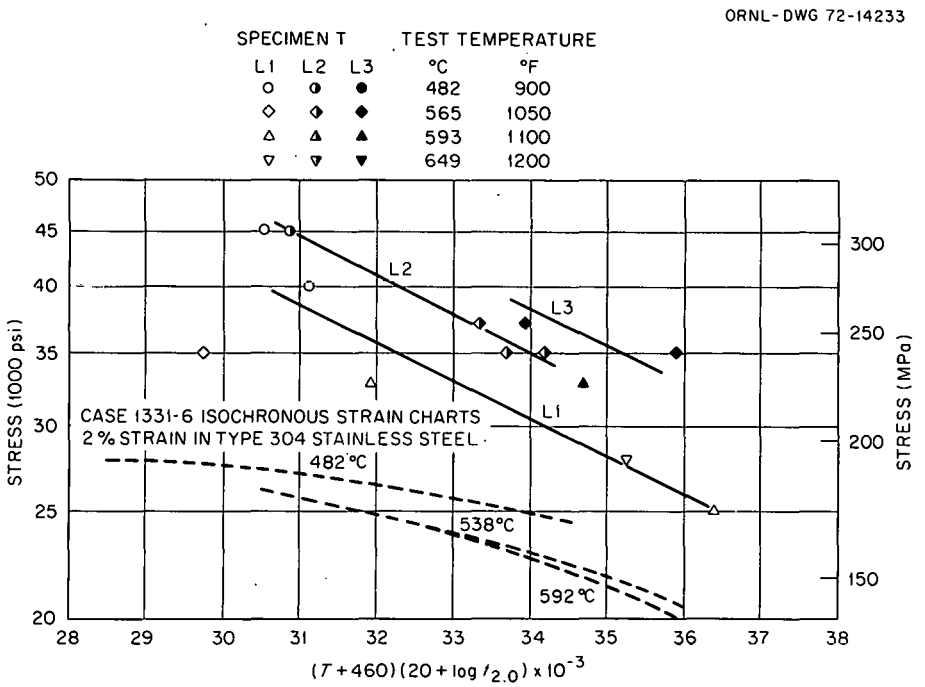

Fig. 5. Stress as a Function of Larson-Miller Parameter for Time to 2% Strain in CRE Type 308 Stainless Steel Weld Metal.

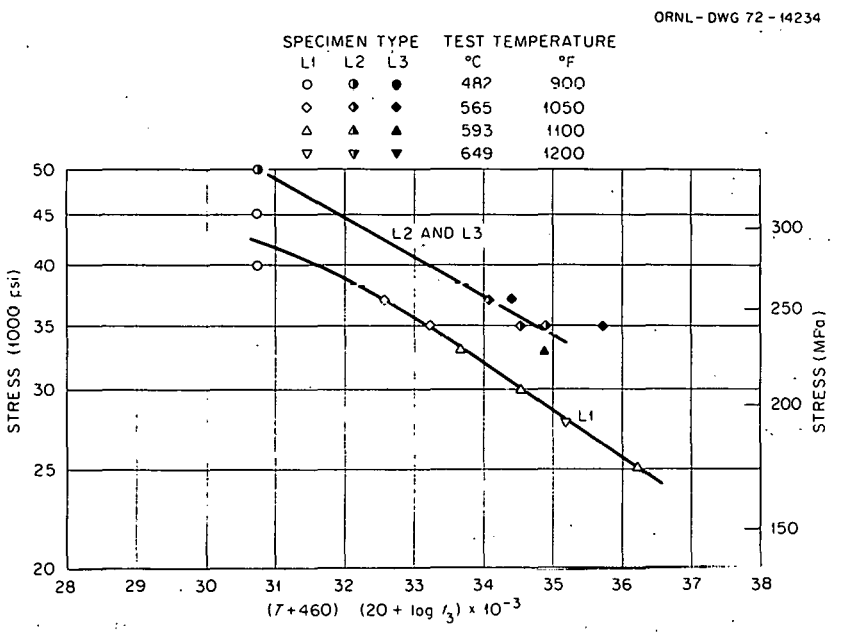

Fig. 6. Stress as a Function of Larson-Miller Parameter for Time to Third-Stage Creep by 0.2% Offset Strain Method for Type 308 Stainless Steel Weld Metal.

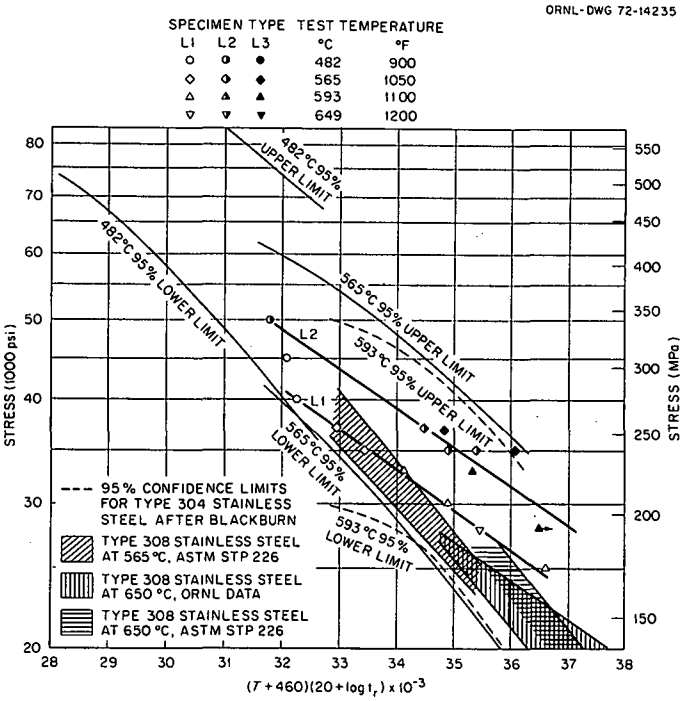

Fig. 7. Stress as a Function of Larson-Miller Parameter for Rupture Time t_r of CRE Type 308 Stainless Steel Weld Metal, Compared with Standard Weld Metal and Type 304 Stainless Steel Base Metal.

included.[14] Different limits are shown for different testing temperatures because the limits were originally derived on other bases than a time-temperature parameter.

Two types of strain data are reported for standard specimens. First, the combined first- and second-stage creep strain (but not including elastic nor plastic loading strain), which is observed at the end of second-stage creep, is plotted against the logarithm of time to rupture in Fig. 8. Both the time and strain values were obtained graphically for a 0.2% strain offset from the minimum creep rate portion of the strain-time curve. Second, the total strain is plotted against the logarithm of the rupture time in Fig. 9. Again, the identity of specimen locations is shown for all tests. Comparisons of the strain-time behavior of longitudinal and transverse standard specimens at 593°C (1100°F) for

[14]L. D. Blackburn, "Isochronous Stress-Strain Curves for Austenitic Stainless Steels," p. 15 in *The Generation of Isochronous Stress-Strain Curves*, ed. by A. O. Schaefer, American Society of Mechanical Engineers, New York, 1972.

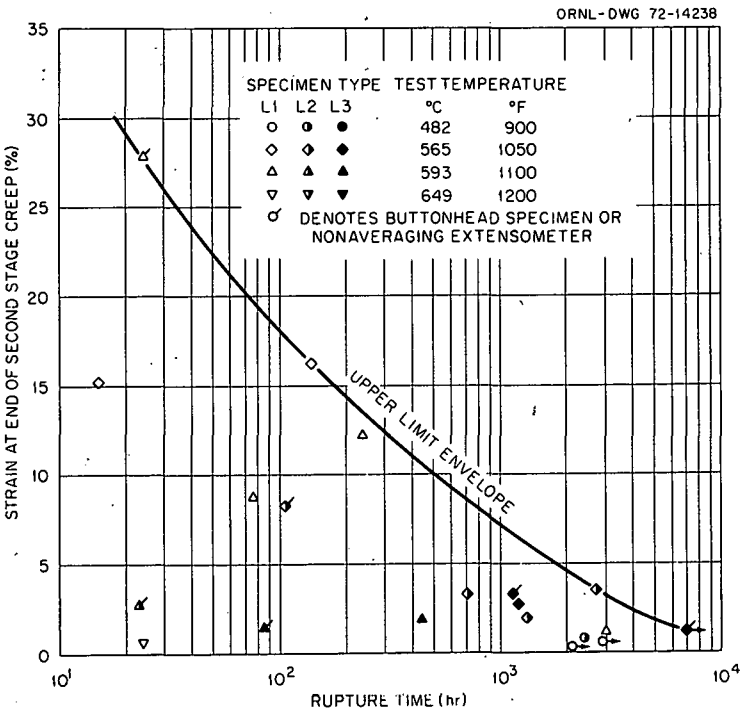

Fig. 8. Approximate First-Stage Plus Second-Stage Creep Strain for CRE Type 308 Stainless Steel Weld Metal.

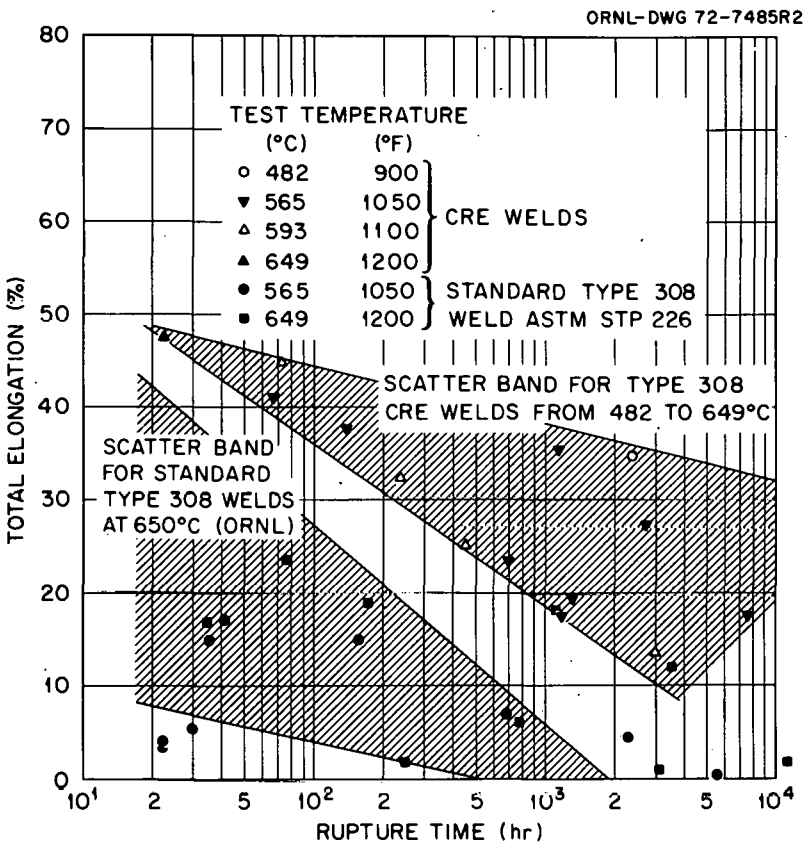

Fig. 9. Ductility in Creep-Rupture Tests of Type 308 Stainless Steel Welds.

230 MPa stress (33,000 psi) are shown in Fig. 10. Direct comparisons may be made between the L1 and T1 specimens and the L3 and T3 specimens. The deformation resistance of the weld metal is different in different directions, even allowing for the presence of base metal from the heat-affected zone in the transverse specimens; transverse specimens are significantly stronger than longitudinal all-weld-metal specimens under these test conditions.

The total elongations and rupture times for the buttonhead specimens tested at 593°C (1100°F) and 240 MPa are mapped in Fig. 11. Failure times for base metal distant from the fusion line range between 100 and 500 hr, and strains all exceed 20%. Base-metal specimens from the heat-affected zone near the fusion line fail in times between 500 and 1200 hr at strains of about 10% or less. All-weld-metal specimens fail in less than 100 hr at strains greater than 20%. The properties of specimens containing the fusion line depend upon the fraction of the gage section that is weld metal.

Microscopy Results

The microstructures of the welds were typical of type 308 stainless steel weld metal containing 5 to 8% ferrite.[15] A continuous austenite matrix separated long, narrow ferrite regions, which were distributed in a cellular dendritic pattern. The substructural boundaries visible in Fig 12(a) are apparently aligned nearly parallel to the solidification direction, and they separate columnar austenite subgrains, which appear to grow epitaxially from the base metal into the weld metal and across inter-pass boundaries in many cases. The ferrite distribution and orientation of the long axes of the grains vary with location within the weld, depending on the solidification growth direction (which, in turn, is controlled by the shape of the molten weld metal puddle during welding).

---

[15]G. M. Goodwin, N. C. Cole, and G. M. Slaughter, "A Study of Ferrite Morphology in Austenitic Stainless Steel Weldments," *Welding J. (Miami)* 51(9): 425s–429s (September 1972).

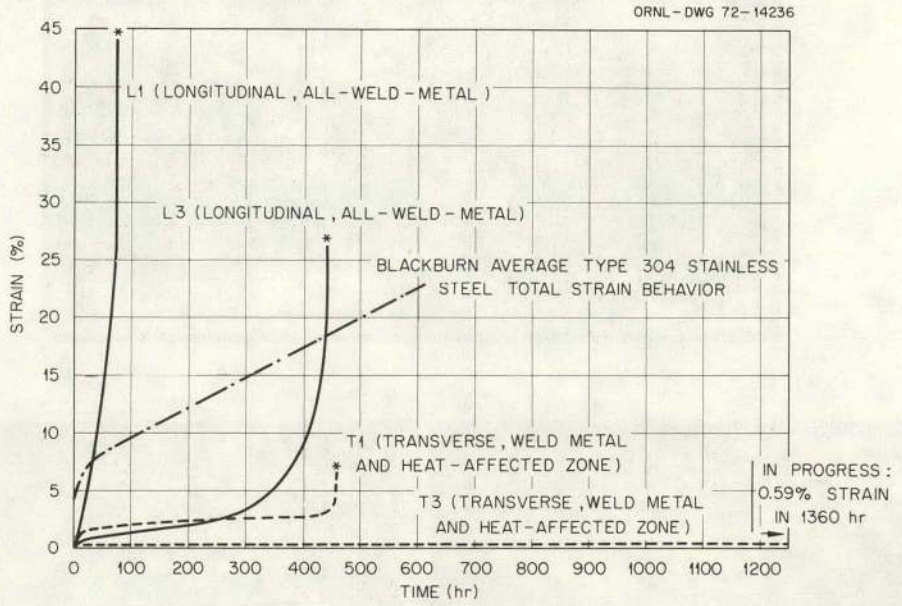

Fig. 10. Comparison of Longitudinal and Transverse Creep Specimens from CRE Type 308 Stainless Steel Weld at 593°C (1100°F) and 230 MPa (33,000 psi). Average data for type 304 stainless steel by Blackburn also plotted.

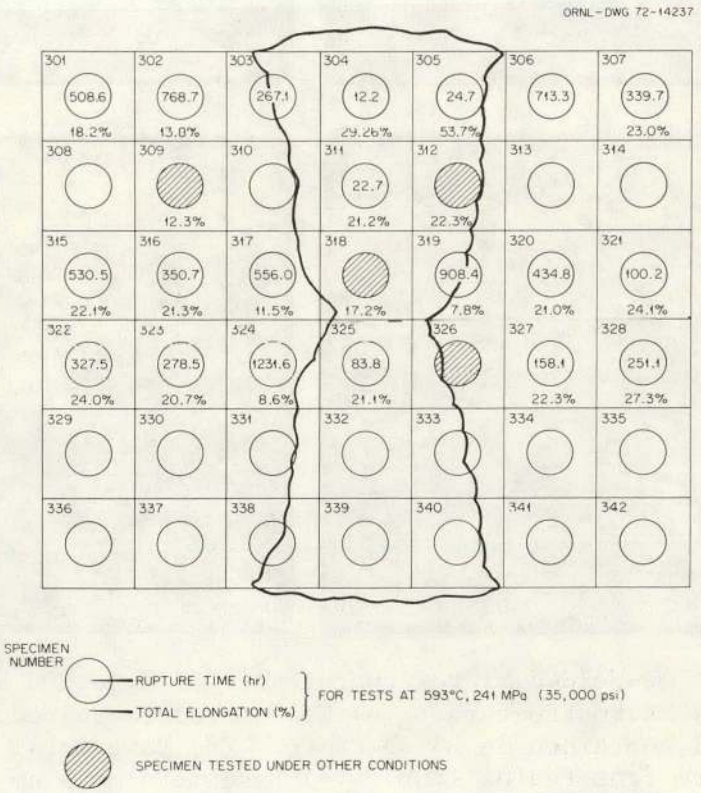

Fig. 11. Map of Rupture Times and Total Elongations for CRE Type 308 Stainless Steel Weld Metal and Type 304 Stainless Steel Base Metal. Hourglass-shaped region is weld metal.

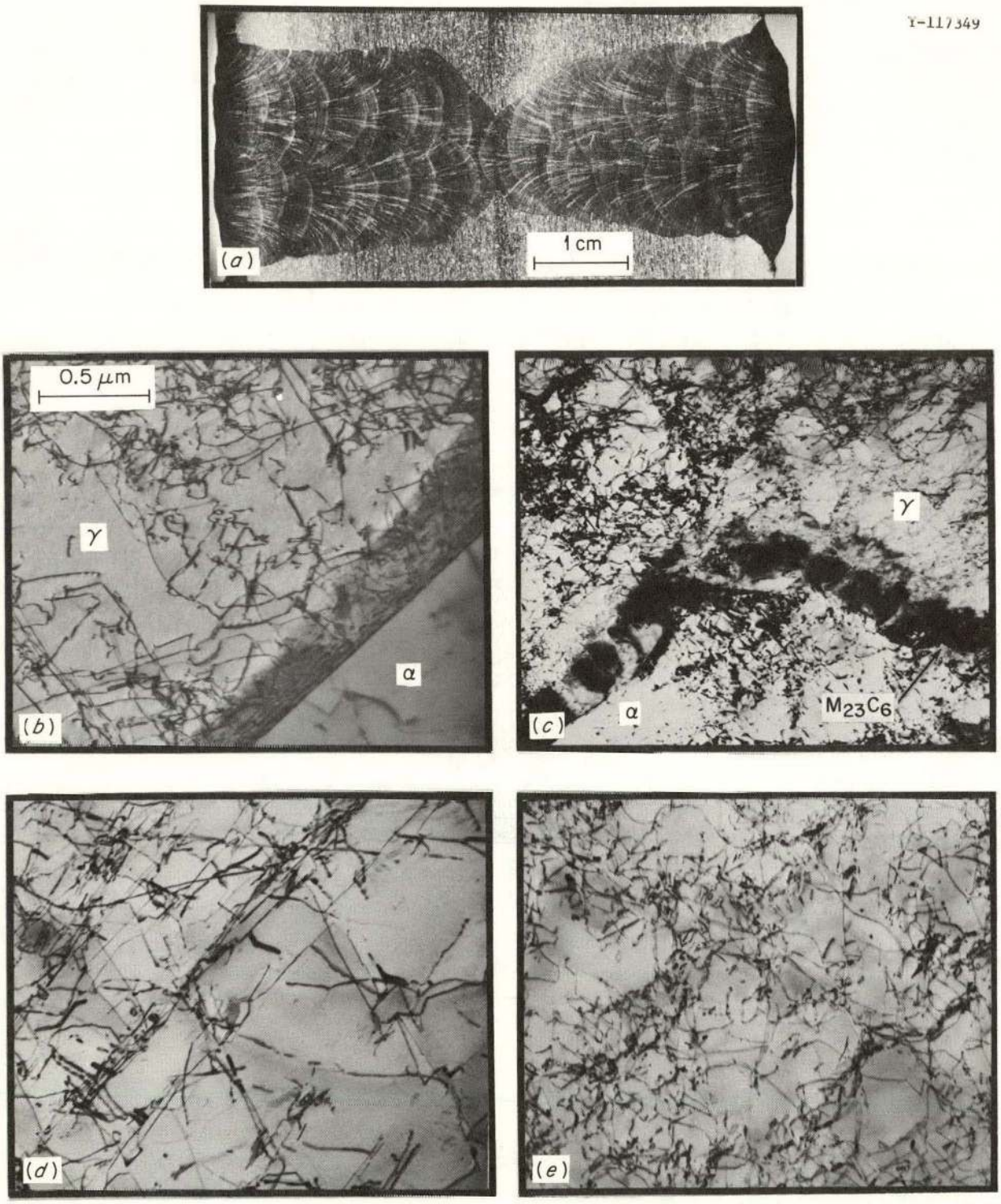

Fig. 12. As-Welded Microstructure of CRE Type 308 Stainless Steel Weldment. (a) Macrostructure. (b) Weld metal contained in L1 specimen. (c) Weld metal contained in L3 specimen. (d) Base metal 1.5 cm below surface, 0.1 cm from fusion line. (e) Base metal 1.5 cm below surface, 1.0 cm from fusion line.

Transmission electron microscopy at 650 kV revealed the systematic variation in the microstructure of the weld metal, shown in Fig. 12(b) and (c). The results are also summarized in Table 2. The austenite phase of weld metal contained in L1 or T1 (surface) specimens had about 1×10^{10} straight dislocations/cm^2 with a poorly developed cell structure; the austenite-ferrite interfaces in this region were free of visible precipitate particles, as seen in Fig. 12(b). Near the center of the weld in a region represented by L3 and T3 specimens, there were about 2.8×10^{10} dislocations/cm^2 arranged in a well-defined cell structure together with some 5.5×10^{15} loops/cm^3. The austenite-ferrite boundaries are nearly covered with $M_{23}C_6$ precipitate. In this region, the particles are massive and their crystallographic orientation is parallel to that of the austenite matrix, as seen in Fig. 12(c). At the intermediate L2 and T2 locations, there were about 2×10^{10} dislocations/cm^2 in the austenite, and the interphase boundaries were decorated with a platelike $M_{23}C_6$ precipitate. The dislocation density in ferrite was generally one-half to one-tenth that in the austenite, but it tended to be highest locally where ferrite widths were small.

Table 2. Defect Statistics in CRE Type 308 Stainless Steel Test Welds, As-Welded Condition[a]

Region	Depth Below Surface (cm)	Phase	Dislocation Density (cm^{-2})	Loop Density (loops/cm^3)	Austenite-Ferrite Interface Precipitate
Weld	0.25	Austenite	1.0×10^{10}	Present[b]	None
Weld	1.5	Austenite	2.05	Present[b]	c
Weld	3.0	Austenite	2.8	5.5×10^{15}	d
Weld	1.5	Ferrite	0.9	Absent	
HAZ[e]	1.5	Austenite	1.6	Present[b]	
HAZ[f]	1.5	Austenite	0.5	Present[b]	

[a] No precipitate in matrix in any specimens.

[b] Not measured.

[c] Platelike $M_{23}C_6$ particles.

[d] Massive $M_{23}C_6$ particles.

[e] Heat-affected zone 0.1 cm from fusion line.

[f] 1.0 cm from fusion line.

The structures of the relatively unaffected type 304 stainless steel base metal and heat-affected zone 1.5 cm beneath the weld surface are shown in Fig. 12(d) and (e), respectively. There was no discontinuity in the dislocation structure at the fusion line. The dislocation density was 1.6×10^{10} dislocations/cm^2 0.1 cm from the fusion line, compared with 0.5×10^{10} dislocations/cm^2 1.0 cm from the fusion line. Near the fusion line, dislocation tangles and cell structures resembled those in the weld metal at a similar distance from the surface. Straight dislocations typical of a light, low-temperature deformation were found 1 cm from the fusion line. No observable precipitate formed in the base metal during welding. These observations are also summarized in Table 2.

The microstructures of CRE type 308 stainless steel weld metal creep specimens all show general elongation parallel to the tensile axis. In the weld metal we observed two reactions whose rates depended on time, temperature, and perhaps strain: the cellular dendritically distributed ferrite in the weld metal transformed to sigma phase during testing, and the $M_{23}C_6$ precipitate dissolved. The transformation to sigma phase has been observed by optical metallography and verified by electron diffraction techniques. No dislocations were ever found in the sigma phase, which is relatively hard.

Surprisingly, internal cracks could not be found in the tested CRE weld metal, even after creep tests lasting several thousands of hours at 593°C (1100°F). Failures occurred by shear and ductile tearing, as evidenced by the dimpled fracture surfaces (Fig. 13). Occassional ledges on the fracture surfaces can be attributed to diversion of the fracture path along weak interphase boundaries, but the predominant mode of fracture propagation in creep tests was not strongly influenced by substructural effects.

DISCUSSION

Properties and Structure of CRE Type 308 Stainless Steel Weldment

The measured local properties of the weld metal and the heat-affected zone are controlled by the welding process. In this multipass weld, metal

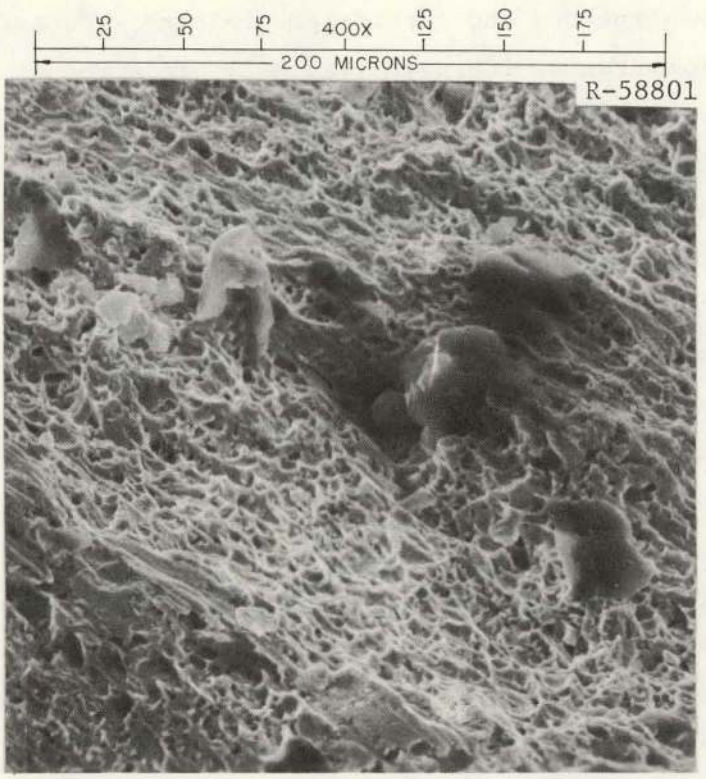

Fig. 13. Scanning Electron Micrograph of CRE Type 308 Stainless Steel Weld Metal Crept to Failure in 2394.6 hr at 482°C. Some oxide scale and embedded inclusions are visible on the fracture surface.

deposited during all but the last pass is subjected to a complex thermo-mechanical history as a result of later weld passes. Solidification shrinkage stresses and thermal stresses[16,17] contribute to relatively heavy deformation of the initial passes, resulting in the high observed dislocation and loop density near the center of the weld. Precipitation of $M_{23}C_6$ at elevated temperatures is a well-known phenomenon in austenitic steels and is sensitive to a number of metallurgical variables, including prior thermal and mechanical treatments.[18] The systematic variations

---

[16]N. T. Williams, C. J. Smith, and L. H. Toft, "Stresses and Strains in Thick Austenitic Steel Plates During Welding," pp. 143–48 in *Proceedings of the Second Commonwealth Welding Conference, April 26–May 16, 1965*, Institute of Welding, London.

[17]A. G. Cepolina and D. A. Canonico, "The Measurement of Residual Stresses," *Welding J. (New York)* 50(1): 31s–38s (January 1971).

[18]B. Weiss and R. Stickler, "Phase Instabilities During High Temperature Exposure of 316 Austenitic Stainless Steel," *Met. Trans.* 3: 851–66 (April 1972).

of dislocation structure and carbide precipitate structure and density through the thickness of the weld (Table 2) are a result of the greater number of thermal and mechanical cycles experienced in the initial passes than in the surface weld passes.

The variation of yield stress with location in the weld (Fig. 2) has been semiquantitatively related to the local density of dislocations in the austenite[19] although other factors, such as local chemical composition, also must affect the yield stress to some degree. The increment in yield stress due to an array of dislocations is proportional to the square root of dislocation density. Although there are no adequate theories relating creep behavior to initial microstructure, the difference in stress required to cause 0.5, 1.0, and 2.0% strain in the L1, L2, and L3 specimens of CRE weld metal (Figs. 3, 4, and 5, respectively) can be ascribed to the observed systematic microstructural variations. In essence, the heavily deformed as-deposited weld metal from the center of the weld is stronger at small strains than weld metal near the surface. This observation is in agreement with the observed yield strength variation. Effects due to second phases and local chemical composition variations are also recognized to have possible importance. The variables are now being investigated in greater detail.

The initial property differences through the thickness of the weld metal persist at larger strains or longer test times. About 20% higher stresses are required to initiate third-stage creep for L3 specimens at a given time-temperature parameter value than are required for L1 specimens (Fig. 6). Similar differences are found for rupture times (Fig. 7).

The total accumulated strain at the end of second-stage creep, including elastic strain, plastic loading strain, first-stage creep strain, and second-stage creep strain, always exceeded 0.5%. However, when the loading strains are not included (Fig. 8), the sum of the first- and second-stage creep strains is less than 0.5% for one long-term 482°C test. The latter strains for all specimens appear to be contained within an

---

[19]R. T. King, J. O. Stiegler, and G. M. Goodwin, "Properties of Thick Type 308 Stainless Steel Welds with Controlled Residual Elements," to be published.

envelope whose upper limit decreases with increasing rupture time. No clear distinction can be made between specimens from different locations, nor are there yet sufficient data to isolate the effect of test temperature.

The lowest observed total strain (Fig. 9) for any all-weld-metal creep specimen of CRE type 308 stainless steel is 13% in tests lasting about one year. All the total strain data are contained in a single scatter band when plotted against rupture time. The band shows decreasing ductility with increasing time to rupture. The available data contain no apparent relationship between specimen location or test temperature and total elongation.

Anisotropy of the deformation characteristics of the weld metal is evident in both the tensile and creep data. The transverse weld metal specimens are consistently stronger than the longitudinal specimens. They are oriented differently with respect to the local solidification substructure. Other work[19] has demonstrated that CRE weld metal deforms relatively easily in the direction parallel to the local substructure, leading to nonuniform diametral reductions similar to those reported for other steel weld deposits.[20] At least two factors directly or indirectly influence anisotropic deformation: the observed preferred crystallographic orientation of the weld metal[21] and the local substructural orientation. The latter factor determines the local orientation of the elongated ferrite phase, the longest mean free path between subgrain boundaries, and, in regions where $M_{23}C_6$ is precipitated, the longest mean free path between walls of hard precipitate particles lying on interphase boundaries. During creep tests the original ferrite phase transforms to sigma phase, and these hard precipitate particles should make deformation more difficult in all directions except parallel to the local substructure. Any or all these factors may contribute to anisotropic deformation under given testing conditions, but the relative importance of each is not yet ascertained.

---

[20] J. Heuschkel, "Anisotropy and Weldability," *Welding J. (New York)* 50(3): 110s–126s (March 1971).

[21] J. Hedger and R. A. Vandermeer, private communication.

The same thermal and stress cycling that contributed to the variations of structure through the as-deposited weld metal is responsible for the variation in properties and microstructure of the nearby type 304 stainless steel base metal. The heat-affected zone of the base metal in the test welds experienced a series of complex thermomechanical cycles during the deposition of successive weld passes. This history had little observable effect on the microstructure except to increase the local dislocation density near the fusion lines, as seen in Fig. 12(d) and (e). However, we recognize that the cycling may influence the stress-aging,[22] which is possible before creep, or dynamic strain-aging processes during creep,[23] both of which affect the properties of austenitic steels. The net effect on properties in the heat-affected zone was to increase the rupture time while decreasing the total elongation relative to the as-received base metal. Note that buttonhead specimens that were part weld metal and part heat-affected base metal exhibited a wide range of properties, depending upon the relative amounts of the ductile, soft weld metal and the less ductile but strong heat-affected base metal in the gage section.

Comparison of CRE Type 308 and Standard Type 308 Stainless Steel Weld Metal Data

The only comparisons that can be made between as-deposited standard type 308 and CRE type 308 stainless steel weld metals are for creep rupture times and total elongations. There are no known published data on the deformation characteristics of standard weld metal at small strains.

Commercial type 308 stainless steel weld metal rupture time data[24] have been plotted in scatter bands by the Larson-Miller parameter in

---

[22]R. H. Harrington, "Stress-Aging and Its Effects on the Standard Tensile Properties of Some Stainless Steels," *Trans. Amer. Soc. Metals* 58: 119–41 (1965).

[23]F. Garafalo, F. Von Gemmingen, and W. R. Domis, "The Creep Behavior of an Austenitic Stainless Steel as Effected by Carbides Precipitated on Dislocations," *Trans. Amer. Soc. Metals* 54: 430–44 (1961).

[24]H. R. Voorhees and J. W. Freeman, *The Elevated-Temperature Properties of Weld-Deposited Metal and Weldments, ASTM Spec. Tech. Publ.* 226, American Society for Testing and Materials, Philadelphia, 1958.

Fig. 7 together with a separate scatter band for ORNL data[25] from the weld development program mentioned previously. The data for L1 specimens of CRE weld metal from near the weld surface fall in or slightly above the scatter bands for standard weld metal. However, the data for L2 and L3 specimens lie above the scatter band, indicating that they have longer rupture times for given test conditions. While this comparison by no means indicates that as-deposited CRE weld metal is superior to all as-deposited type 308 stainless steel weld metal, its creep rupture strength is at least as great as or greater than reported values presently available.

The total elongations of CRE weld metal at various rupture times are compared with ductility data from the same sources[24,25] in Fig. 9. With the exception of one datum for standard weld metal, all the elongations for standard weld metal lie within an envelope whose upper bound is the bottom of the scatter band representing the ductility of CRE weld metal. An extrapolation of the envelope approaches zero total strain for standard weld metal at about 10,000 hr rupture time. On the other hand, although the scatter band for CRE weld metal indicates decreasing rupture strain for long rupture times, no strain less than 13% has been recorded for tests lasting up to 7550 hr, and it is not certain whether the CRE all-weld-metal specimen ductility will approach the nil value even for longer times and higher test temperatures.

The differences in ductility between the standard and CRE weld metal can be related to differences in the fracture mode. For long-time creep rupture at 649°C (1200°F), the fracture in standard weld metal frequently initiates at original austenite-ferrite boundaries and the final fracture links these internal cracks.[26,27] The transformation of ferrite to sigma phase and dissolution of carbide occur under these test conditions[28] and

---

[25] G. M. Goodwin, N. C. Binkley, N. C. Cole, and R. G. Bergren, *Metals and Ceramics Div. Annu. Progr. Rep. June 30, 1971,* ORNL-4770, pp. 82–85.

[26] G. M. Slaughter, N. C. Binkley, G. M. Goodwin, D. G. Harman, and N. C. Cole, *Metals and Ceramics Div. Annu. Progr. Rep. June 30, 1970,* ORNL-4570, pp. 88–91.

[27] G. M. Goodwin, N. C. Cole, and G. M. Slaughter, "A Study of Ferrite Morphology in Austenitic Stainless Steel Weldments," *Welding J. (Miami)* 51(9): 425s–429s (September 1972).

[28] J. O. Stiegler, R. T. King, and G. M. Goodwin, "Fracture Mechanisms in Austenitic Stainless Steel Weld Metal," to be published.

at other temperatures and times with different reaction kinetics,[29] providing a variety of interphase boundaries to serve as fracture paths, which parallel the macroscopic austenite-ferrite boundaries. Extensive sigma phase—austenite boundary separations, which initiate fracture and result in the observed fracture morphologies, have been identified in standard type 308 stainless steel weld metal.[28]

Conversely, the interphase boundaries in CRE type 308 stainless steel weld metal have not been observed to separate internally during creep tests. The predominantly shear fracture surfaces occasionally are diverted along substructural features, but no metallographic or electron-microscopic evidence for fracture initiated by internal cracking has been found. All of the types of interphase boundaries found in standard weld metal also exist in the CRE weld metal.

Weldment Behavior at Elevated Temperatures and Design Considerations

A goal of this work is to provide data enabling designers to predict the behavior of weldments at elevated temperatures. Two separate situations must be considered: first, that for existing design rules governing nuclear components,[30] and second, a more detailed analytical approach in which all of the physical characteristics of welds are properly accounted for. Type 308 stainless steel weld metal joining type 304 stainless steel base metal will be considered as an example.

The CRE type 308 stainless steel all-weld-metal data show higher strength than the average values for type 304 stainless steel. The stresses required to produce 0.5, 1.0, and 2.0% strain in base metal have been plotted in Figs. 3, 4, and 5, respectively, against the Larson-Miller time-temperature parameter derived from the isochronous stress-strain curves at 482, 538, and 592°C (900, 1000, and 1100°F). From these three

---

[29]B. Weiss and R. Stickler, "Phase Instabilities During High Temperature Exposure of 316 Austenitic Stainless Steel," *Met. Trans.* 3: 851—66 (April 1972).

[30]Case 1331-6, *Interpretations of ASME Boiler and Pressure Vessel Code*, American Society of Mechanical Engineers, New York, 1972.

plots, the strengths of weld metal can be compared with average expected values for base metal at small strains. Stresses required to cause failure of CRE weld metal for a given rupture time and temperature (Fig. 7) lie within the 95% confidence limit band for type 304 stainless steel base metal. The acceptable strength of the CRE weld metal combined with good ductility (Fig. 9) make it a viable weld metal from the standpoint of creep properties by present rules.

However, a great deal of effort is presently being directed toward understanding the behavior of weldments in greater detail. Numerical finite element analyses of the stress-strain state during welding[31] and of weldments during deformation[32-36] have shown nonuniformity of stress and strain distributions in weldments when the various regions in and near welds are treated as homogeneous, isotropic media. Quite clearly, an accurate description of the real weldment investigated here would require continuously varying mechanical properties throughout the weld metal and heat-affected region and the inclusion of anisotropic deformation characteristics for the weld metal, with a point-to-point variation in the

---

[31]H. D. Hibbih and P. V. Marcal, "A Numerical, Thermo-Mechanical Model for the Welding and Subsequent Loading of a Fabricated Structure," to be published.

[32]S. K. Chan, M. J. Manjoine, and C. Visser, *Analysis of Stresses in Pressurized Welded Pipe in the Creep Range*, ASME 71-PVP-66, American Society of Mechanical Engineers, New York, 1971.

[33]D. J. Walters and R.D.H. Cockroft, "A Stress Analysis and Failure Criteria for High Temperature Butt Welds," paper presented at the International Institute of Welding Colloquium on Creep Behavior of Welds in Boilers, Pressure Vessels, and Pipelines, Toronto, 1972.

[34]C.H.A. Townley, I.W. Goodall, and D. J. Lewis, "Design Criteria for Welded Pressure Parts," paper presented at International Conference on Welding Research Related to Power Plant, September 17–21, 1972, Central Electricity Generating Board Marchwood Laboratories, England.

[35]A. K. Hardy, I. W. Goodall, and T. Rowley, "Design and Operational Aspects of Steam Pipe Transition Joints," paper presented at International Conference on Welding Research Related to Power Plant, September 17–21, 1972, Central Electricity Generating Board Marchwood Laboratories, England.

[36]E. Chubb, R. Fidler, and D. Wallace, "Development and Relaxation of Welding Stresses," paper presented at International Conference on Welding Research Related to Power Plant, September 17–21, 1972, Central Electricity Generating Board Marchwood Laboratories, England.

orientation of the principal axes of anisotropy. Design criteria based on the behavior of the most highly stressed or strained element of the weld metal or base metal might then be developed.

SUMMARY

The creep properties of a shielded metal arc, multipass, type 308 stainless steel pressure-vessel test weld between 482 and 650°C (900 and 1200°F) have been investigated to obtain design data. The particular weld contained controlled amounts of the residual elements B (0.007%), Ti (0.06%), and P (0.04%) and is designated controlled residual elements (CRE). Results of the investigation showed the following for as-deposited weld metal and heat-affected zones:

1. Systematic variations in microstructure occur through the thickness of the weld. In the initial passes at the center of the weld dislocation densities are highest, dislocation loops form, cell structures form, and $M_{23}C_6$ precipitates on austenite-ferrite interfaces as a result of numerous thermal and mechanical cycles experienced during welding. The carbide precipitate density, loop density, and dislocation density decrease gradually toward the surface of the weld, where less thermal and mechanical cycling occurred. Near the surface proper, few dislocation loops and no precipitate are present, and the dislocation density is about 2.8 times lower than near the center of the weld. The dislocations near the surface are generally straight, and only a hint of crude cell structure occurs.

2. Systematic variations in creep properties at small and large strains are at least partly attributable to these microstructural variations. Weld metal from initial passes is stronger than weld metal in the final passes.

3. Dislocation densities in base metal from the heat-affected zone increase near the fusion line. Due to the complex thermal and mechanical cycling, type 304 stainless steel base metal from near the fusion line is stronger but less ductile than base metal unaffected by welding.

4. Anisotropic deformation occurs and is influenced by the local substructural orientation, preferred crystallographic orientation, or both;

since these orientations vary throughout the weld, the principal axes of anisotropy also vary with location. Transverse specimens are stronger in creep than longitudinal, all-weld-metal specimens under the test conditions explored.

5. Internal cracks did not develop at interphase boundaries of CRE weld metal. The ductility of CRE weld metal is superior to published results for standard type 308 stainless steel weld metal, which does crack internally at interphase boundaries.

6. The creep strength of CRE weld metal is as good as or better than creep strength published for standard type 308 stainless steel weld metal.

7. The creep strength properties of CRE type 308 stainless steel weld metal satisfy the requirements of present nuclear pressure-vessel design codes over the range of temperatures and stresses investigated.

ACKNOWLEDGMENTS

The authors wish to thank E. Bolling, J. K. Alley, and S. W. Cook for their diligent efforts on the experimental work. Gratitude is also expressed to E. W. Pickering, Jr., J. F. Turner, and C. T. Ward for their efforts in preparing the test welds. The authors thank F. R. Cox and C. A. Stephens for preparing the manuscript, and S. Peterson for his diligent editorial work. The encouragement of and fruitful discussions with P. Patriarca, J. R. Weir, Jr., W. R. Martin, H. E. McCoy, G. M. Slaughter, N. C. Cole, D. A. Canonico, and R. G. Berggren are gratefully acknowledged.

THIS PAGE

WAS INTENTIONALLY

LEFT BLANK

ORNL-TM-4131
UC-79b — Liquid Metal Fast Breeder Reactors
(Fuels and Materials Engineering and Development)

INTERNAL DISTRIBUTION
(116 copies)

(3) Central Research Library
ORNL — Y-12 Technical Library
Document Reference Section
(10) Laboratory Records Department
Laboratory Records, ORNL RC
ORNL Patent Office
G. M. Adamson, Jr.
S. E. Beall
R. G. Berggren
E. E. Bloom
D. A. Canonico
R. W. Carpenter
R. E. Clausing
J. A. Conlin
W. A. Coughlan
N. C. Cole
J. M. Corum
R. S. Crouse
F. L. Culler
J. E. Cunningham
J. H. DeVan
R. G. Donnelly
D. Fahr
K. Farrell
M. H. Fontana
J. H Frye, Jr.
W. R. Gall
G. M. Goodwin
R. J. Gray
B. L. Greenstreet
W. O. Harms
(5) M. R. Hill
D. O. Hobson
F. J. Homan
H. Inouye
P. R. Kasten
(5) R. T. King
R. L. Klueh
R. W. Knight
J. W. Koger
B. C. Leslie
K. C. Liu
E. L. Long, Jr.
A. L. Lotts
M. I. Lundin
R. N. Lyon
R. E. MacPherson
W. R. Martin
C. L. Matthews
A. J. Moorhead
W. J. McAfee
H. E. McCoy, Jr.
H. C. McCurdy
C. J. McHargue
E. L. Nicholson
P. Patriarca
C. E. Pugh
P. L. Rittenhouse
W. K. Sartory
J. L. Scott
J. D. Sease
G. M. Slaughter
W. J. Stelzman
(5) J. O. Stiegler
R. W. Swindeman
D. B. Trauger
W. E. Unger
R. E. Vandermeer
T. N. Washburn
J. R. Weir, Jr.
G. D. Whitman
F. W. Wiffen
J. W. Woods
M. H. Yoo

Subcontractors and Consultants

Atomic International, P. O. Box 309, Canoga Park, CA 91304

R. I. Jetter

Babcock & Wilcox Company, P. O. Box 835, Alliance, OH 44601

W. E. Leyda
C. C. Schultz
D. B. Van Fossen

Battelle Memorial Institute, 505 King Ave., Columbus, OH 43201

C. E. Jaske
E. C. Rodabaugh
G. H. Workman

Brown University, Providence, RI 02912

W. N. Findley

The Catholic University of America, Washington, DC 20017

A. J. Durelli

Cornell University, Department of Materials Science and Engineering, Ithaca, NY 14850

G. V. Smith

E. P. Esztergar, 7993 Prospect Place, La Jolla, CA 92037

Franklin Institute Research Laboratories, The Benjamin Franklin Parkway, Philadelphia, PA 19103

Zenons Zudans

General Electric Company, 175 Curtner Ave., San Jose, CA 95125

Y. R. Rashid

Pennsylvania State University, University Park, PA 16802

S. Y. Zamrick

Teledyne Materials Research Company, 303 Bear Hill Road, Waltham, MA 02154

T. Branca
W. E. Cooper
J. L. McLean

University of California, Lawrence Radiation Laboratory, Inorganic Materials Research Division, Berkeley, CA 94720

Leo Brewer

University of California, Revelle College, Department of Physics, P. O. Box 109, La Jolla, CA 92037

Walter Kohn

University of Illinois, Department of Physics, Urbana, IL 61801

W. S. Williams

EXTERNAL DISTRIBUTION
(206 copies)

USAEC DIVISION OF REACTOR DEVELOPMENT AND TECHNOLOGY, Washington, D.C. 20545

(2) Director

USAEC-RDT SENIOR SITE REPRESENTATIVE, Oak Ridge National Laboratory, Oak Ridge, TN 37830

USAEC OAK RIDGE OPERATIONS OFFICE, P. O. Box E, Oak Ridge, TN 37830

Research and Technical Support Division

USAEC TECHNICAL INFORMATION CENTER, Office of Information Services, P. O. Box 62, Oak Ridge, TN 37830

(202) For distribution as shown in TID-4500 Distribution Category, UC-79b, Liquid Metal Fast Breeder Reactors (Fuels and Materials Engineering and Development)